Cloud-Aerosols interactions by multiple scenarios approach

Eduardo Landulfo, Jonatan J. da Silva, Fábio J. S. Lopes

Eduardo Landulfo, Jonatan J. da Silva, Fábio J. S. Lopes, "Cloud-Aerosols interactions by multiple scenarios approach," Proc. SPIE 10424, Remote Sensing of Clouds and the Atmosphere XXII, 104240Z (20 October 2017); doi: 10.1117/12.2278588

SPIE.

Event: SPIE Remote Sensing, 2017, Warsaw, Poland

Cloud-Aerosols interactions by multiple scenarios approach

Eduardo Landulfo[a], Jonatan J. da Silva[a,b], and Fábio J. S. Lopes[a]

[a]Instituto de Pesquisas Energéticas e Nucleares (IPEN/CNEN-SP), São Paulo, Brasil
[b]Universidade Federal do Oeste da Bahia (UFOB), Bahia, Brasil

ABSTRACT

Aerosols can play the role of cloud and ice condensation nuclei. This study shows a set of measurements and experiments analysis in remote sensing, in distinct scenarios of cloud cover during day/nightime measurements using lidar, visible all-sky camera and solar photometry. The retrieved products are studied to obtain aerosol optical and physical properties in the vicinity of clouds. In this approach cloud cover and optical properties should be retrieved as well as main features used for cloud pixel identification, e. g., Red-Blue Difference, Red-Blue Ratio, Normalized Red-Blue Ratio, Saturation and Intensity. We show some case studies to illustrate this methodology.

Keywords: Lidar measurements, aerosol optical depth, cloud cover, cloud ratio

1. INTRODUCTION

In order to forecast and understand better climate changes one has to quantify with good precision and accuracy the aerosol particles impact. These particles might be of natural or anthropic sources. The most important aspect is how these particles can affect cloud microphysics? Atmospheric aerosols go through many processes such as coagulation, phase transition, gas absorption and ultimately chemical reactions, which might occur in clouds, formed by coagulation of water vapor with pre-existing particles called condensation nuclei and ice nuclei.[1] Retrieved digital camera sky images can be used to classify cloud coverage as clear, cloudy or undefined. In these images clouds are usually displayed in white and grey colors denoting Lorentz-Mie scattering by cloud particles in the solar visible spectrum. A cloud-free sky will be displayed in blue tones denoting molecular Rayleigh Scattering. The algorithms developed to cloud detection use these scattering properties. A direct advantage of the use of the Fixed Threshold (FT) method is the short computation time to make pixel classification. Koehler et al.[2] apply two limit values to Red-Blue ratio in a R-B space to distinguish among opaque and thin clouds and clear sky image obtained when working with equipments such as Whole Sky Imagers (WSI). On the same reasoning, Long et al.[3] and Heinle et al.[4] suggest a single threshold value of 0.6 to classify pixels in a cloudy sky in R-B space. All sky-camera retrieves images based on Sun irradiance information. The irradiance information is important and can be applied when one wants to retrieve Aerosol Optical Depth (AOD), as well as cloud detection.[5]

2. INSTRUMENTS

The lidar system called MSP-Lidar I, and named as SPU (**S**ao **P**a**U**lo) (https://gawsis.meteoswiss.ch/GAWSIS//index.html#/search/station/stationReportDetails/949) lidar station according to **G**lobal **A**tmosphere **W**atch (GAW-WMO) system (http://www.wmo.int/pages/prog/arep/gaw/gaw_home_en.html), is located at Center for Lasers and Applications (CLA) of the Nuclear and Energy Research Institute (IPEN) (Lat : $23.56^\circ S$ and $Long$: $46.74^\circ W$, 740 m above sea level), in the western region of São Paulo city. The SPU lidar station is a multiwavelength Raman lidar operating since 2001.[6,7] It is configured in a monostatic biaxial alignment pointing vertically to the zenith. The transmission system consists of a pulsed Nd:YAG with fundamental emission at 1064 nm. Additional emissions at 532 and 355 nm are obtained from second and third harmonic generators. The

Further author information: (Send correspondence to Eduardo Landulfo: Eduardo Landulfo: E-mail: landulfo@gmail.com, Telephone: +55 (11) 3133 9372

Remote Sensing of Clouds and the Atmosphere XXII, edited by Adolfo Comerón, Evgueni I. Kassianov, Klaus Schäfer, Richard H. Picard, Konradin Weber, Proc. of SPIE Vol. 10424, 104240Z
 · doi: 10.1117/12.2278588

backscattered signal is collected by a 30 cm-diameter Newtonian telescope and split into six spectral channels using dichroic mirrors and interference filters. The detection and spectral selection is performed at these six channels corresponding to elastic wavelengths at 1064, 532 and 355 nm, and traditional channels for the Raman signals at 607 nm and 387 nm (N_2 Raman-shifted signal from 532 nm and 355 nm) and 408 nm (water vapor Raman-shifted signal from 355 nm). The instrument is operating with a vertical spatial resolution of 7.5 m. Since 2008 the SPU lidar station is part of LALINET (http://lalinet.org), that is a coordinated lidar network focused on the vertically-resolved monitoring of the particle optical properties distribution over Latin America.[8,9] The AErosol RObotic NETwork (AERONET)[10,11] is an international system of ground-based sun photometers that provides automatic sun and sky scanning measurements. Using direct sun measurements, AERONET provides both AOD and the Angström Exponent (Å), which gives the wavelength dependence of the AOD. By using multiangular and multispectral measurements of atmospheric radiance and applying a flexible inversion algorithm, the AERONET data can also provide several additional aerosol optical and microphysical parameters, such as size distributions, single-scattering albedo and refractive index. The operating principle of this system is to acquire aureole and sky radiance observations using a large number of solar scattering angles through a constant aerosol profile, and thus retrieve the aerosol size distribution, the phase function and the AOD. An Automated Sky Imaging System (ASI) model J1006 (CMS Schreder Gmbh)[12] was installed in our lidar station facility practically colocated with the lidar system. This system is made up of an all-sky camera (fisheye lenses) and a proprietary software for data acquisition and analysis for a 5 minute cycle after which the obtained images are transmitted and recorded in a remote computer. These sky images are recorded in JPEG files with 1600 by 1200 pixels.

3. METHODOLOGY

In this study, initially two sets of images were visually selected as patterns for clear and cloudy skies in order to set up a cloud cover classification method. The thresholds applied in the analysis were two, a clear sky situation and dark set post processed thresholds. The selected days are those which could be provided by all instruments, the all-sky camera, the lidar system and the sunphotometer which belongs to AERONET. The images inserted in the lower-right corner of figure 1 were retrieved by all-sky camera at solar zenital angles of 37.7° and 45.1°, respectively, and show the time for the profile analysis in order to obtain the correspondent backscattering profiles and total column lidar ratio tuned by the AOD provided by AERONET sunphotometer. The two thresholds parameters for analysis are presented in figure 1.

The image pixel classification can be easily achieved by applying fixed thresholds to RGB components and their correlation instead of directly applying them to the image RGB components.[13] Many parameters have been suggested for image pixel classification, the following table 1 summarizes these parameters usually used in cloud detection algorithms.

Sky physical properties are described by 5 different parameters. In fact Rayleigh molecular scattering changes with the inverse wavelength fourth power and therefore blue light is more scattered than red light in the atmosphere, while cloud particles scatter them equally and from that clouds appear white or grey when absorption and multi-scattering are taken into account.

The retrieved parameters in this approach were: Red-Blue Ratio (RBR), Normalized Red-Blue Ratio (NRBR), Red-Blue Difference (RBD), Blue-Green Difference (BGD), Blue-Red Blue-Green Ratio (BRBG), Saturation and Euclidean Distance. In figure 2 are presented the results of post processed digital images for a example of clear sky data.

The fixed threshold is limited by atmospheric conditions as we use a set of values to refine our selection criteria, in such a way we can classify the images as: clear, cloudy and undetermined. The set of parameters with the least variance were chosen as threshold. As observed, the cloud cover classification task shows difficulties near circumsolar regions and close to the horizon as the Mie scattering intensifies. This is observed in figure 3 by perfor

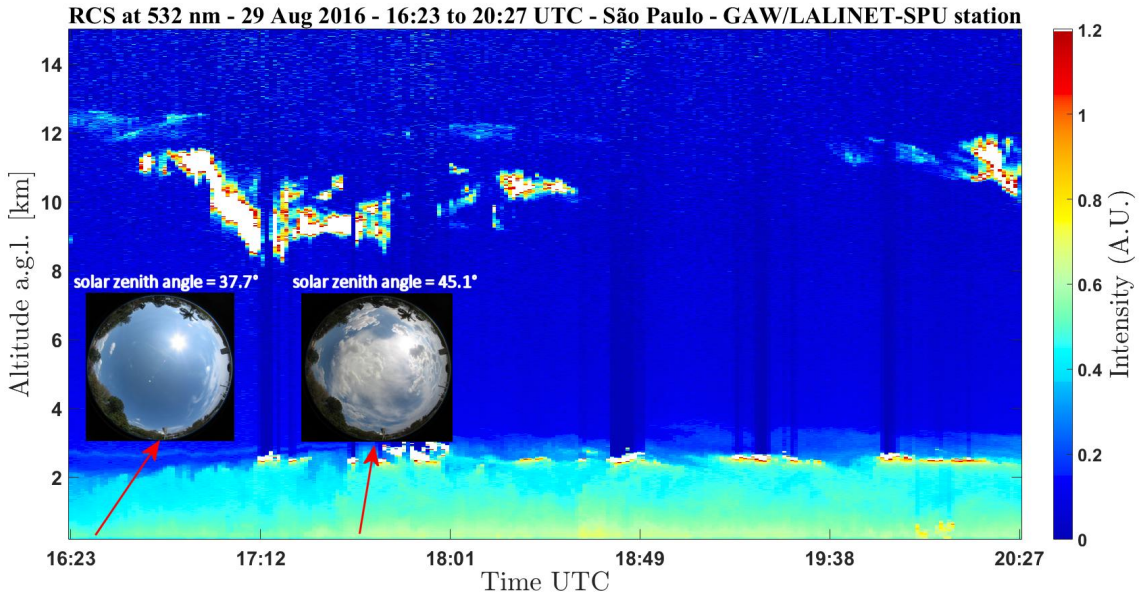

Figure 1. Range corrected signal (RCS) at 532 nm retrieved by the GAW/LALINET SPU lidar station at 29^{th} of August of 2016. The inserted images from the all-sky camera are related to the analyzed period presented in this study.

Table 1. Main parameters used in image pixel identification of clouds.

Parameter	Equation	References
Red-Blue Ratio (RBR)	$RBR=\frac{R}{B}$	[3,12]
Blue-Red Blue-Green Ratio (BRBG)	$BRBG=\frac{B}{R}+\frac{B}{G}$	14
Red-Blue Difference (RBD)	$RBD=R-B$	4
Blue-Green Difference (BGD)	$BGD=B-G$	4
Normalized Red-Blue Ratio (NRBR)	$NRBR=\frac{R-B}{R+B}$	[15 - 16]
Saturation	$Sat=1-\frac{min(R,G,B)}{max(R,G,B)}$	[17 - 18]
Euclidean Geometric Distance (EGD)	$EGD=\sqrt{R^2+G^2+B^2+\frac{(R+G+B)^2}{3}}$	[17,19,20]

The so called classical methods which use a fixed threshold may lead sometimes to wrong conclusion as one can see in figure 3, where 0.1214% of the selected images are sampled as cloudy 2.306% as undetermined. Even with this limitation as a result of the increase of radiation scattering at sunrise and sunset it is still possible to classify 95.35% of images as clear sky conditions.

The classification results for a set of digital images visually selected as cloudy show a good matching among the images, as can be seen in figure 4. The fixed threshold method applied to this set has correctly classified 97.57% of images as cloudy and those images identified as clear and undetermined occur mainly during sunrise and sunset.

4. RESULTS

We have selected two days as a case study, namely 29^{th} August and 12^{th} September, both dates during 2016, in which we have carried on measurements with a SPU lidar station, sunphotometer and the all-sky camera. These days are part of a larger campaign carried on in the second semester of 2016 and correspond to the winter

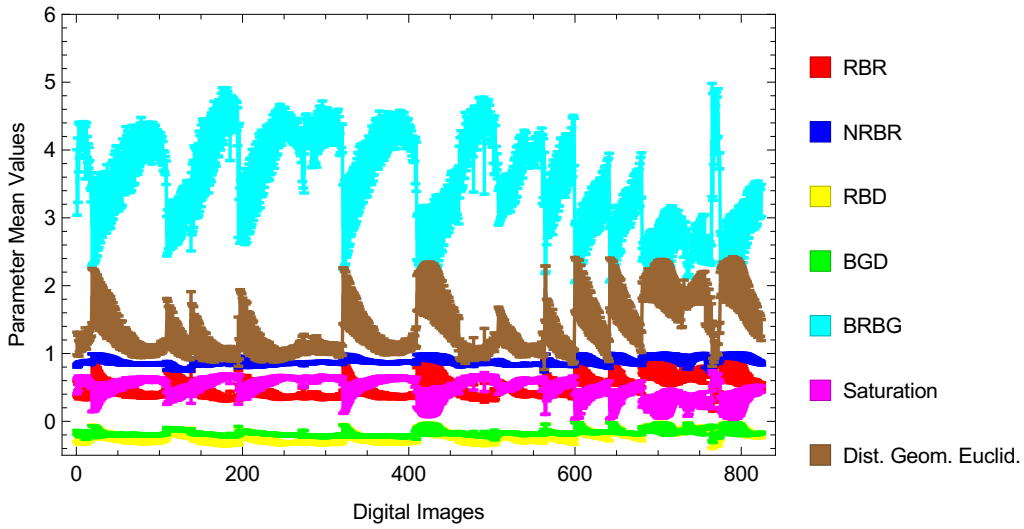

Figure 2. Retrieved parameter by post processed digital images of a set visually classified as clear sky conditions.

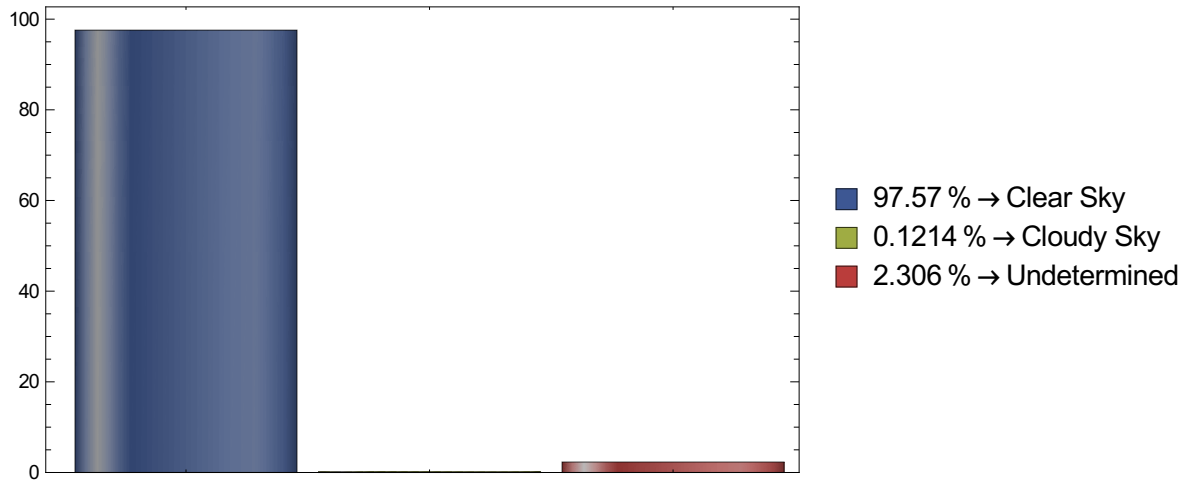

Figure 3. Digital image classification for cloudy and software undetermined days which are affected by the limitation on the fixed threshold method applied to a set of images visually classified as clear sky conditions. Images chosen between 08/16 and 09/23/2016.

(dry) season on the South hemisphere, mostly characterized by frequent cold fronts which cause changes in the aerosol distribution over the Metropolitan Region of São Paulo, and by the detection of transportation of biomass burning plumes from the Central-Western region of Brazil.[21]

4.1 AOD effect on Red-Blue Ratio

4.1.1 Acquisition day - 29th of August, 2016

The AOD variation has impact in the all-sky camera RGB channel intensities, in this sense, some analysis was conducted by comparison of image RBR with interpolated AERONET AOD's at 532 nm, τ_{532}. The images

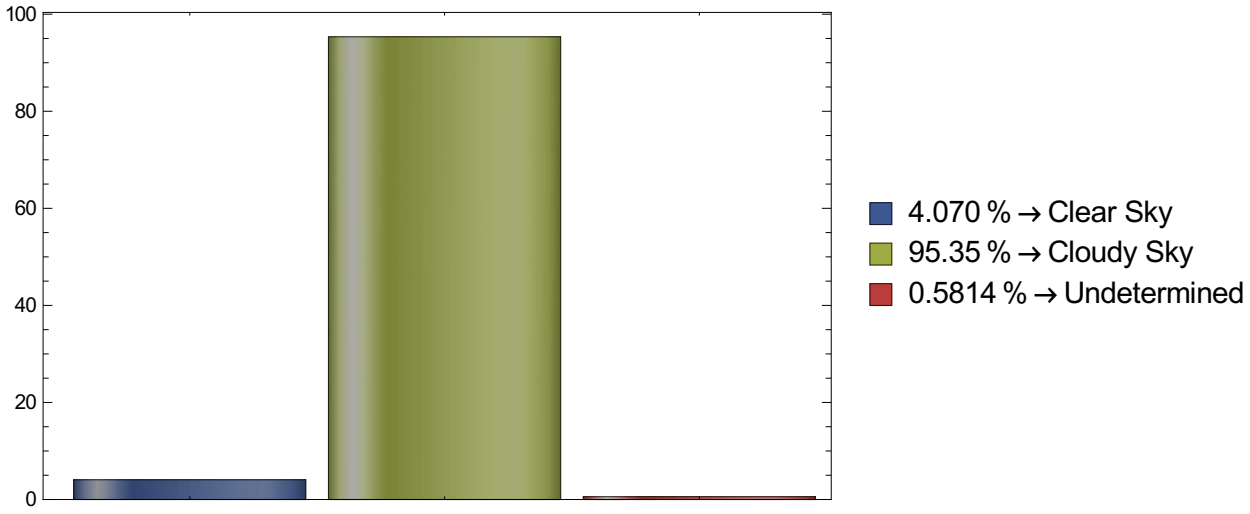

Figure 4. Applying the digital image classification, clear sky conditions and undetermined misclassification occur as the fixed threshold method is applied to cloudy visually classified images. Images chosen between 08/18 and 09/03/2016.

inserted in the lower-right corner of figure 1 were retrieved by all-sky camera at solar zenital angles of 37.7° and 45.1°, respectively, and show the time for the profile analysis in order to obtain the correspondent backscattering profiles and total column lidar ratio tuned by the AOD provided by AERONET sunphotometer. In our case, the all-sky camera and sunphotometer are a short distance apart, about 350 meters. Two days are selected to be analyzed, 29^{th} of August and $12^{th}$of September of 2016, when all-sky images were retrieved together with sunphotometer and lidar data. The cloud covering was not high during these days, allowing measurements with lidar in clear sky and cloudy conditions. The all-sky camera images were retrieved every 5 minutes while sunphotometer data were retrieved every 15 minutes.

The RBR for each image was calculated for situations when the Sun angles were between 30° and 70°. The RBR-AOD correlation for 29^{th} of August shows a linear dependence between these quantities, as can be seen in figure 5.

The mean RBR values retrieved by all-sky images were compared with the AERONET AOD values at 532 nm, for the closest measurement in time ($\approx$ 4 min). The RBR-AOD correlation for the case study of 29^{th} of August of 2016 was:

$$RBR \;=\; 0.5837 \;+\; 0.3206\,\tau_{532} \tag{1}$$

This particular case of 29^{th} of August presents a considerable cloud cover during some periods, as can be observed in the range corrected signal at 532 nm (RCS at 532 nm) retrieved by the SPU lidar station, presented in figure 6. It also presented the 532 nm backscatter profile retrieved applying the Klett-Fernald inversion process[22–24] for two different scenarios. The first one by under clear-sky conditions, before the cloud formation at the top of the Planetary Boundary Layer (PBL), and the second scenario is for the case after and during the cloud detection at the top of the PBL as can be seen in bottom left and right panel of figure 6, respectively. The lidar profiles slightly change between altitudes of 2000 and 3000 m, just in the cloud formation region. From the first scenario, the PBL by around 2400 meters of altitude and there is a thin aerosol layer between 2700 to 2800 meters, as can be seen in the bottom-left panel of figure 6. The column integrated lidar ratio LR for this cloud free scenario is ($LR = 65 \;\pm\; 13$ sr). After some cloud detection there are some small changes in the backscatter lidar profile. The PBL height is around 2800 meters and the thin aerosol layer detected before, in

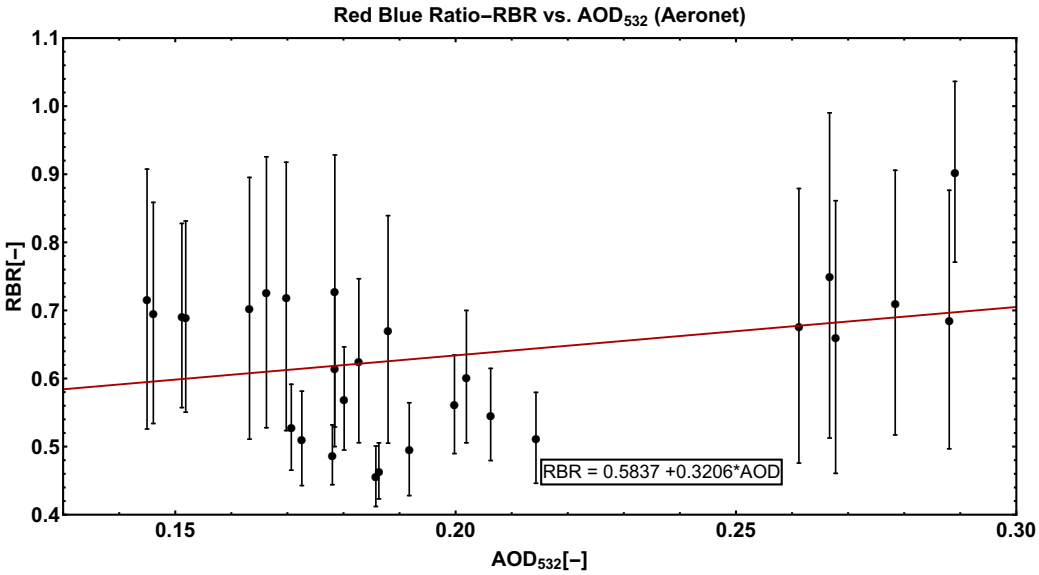

Figure 5. RBR-AOD at 532 nm correlation for 29^{th} of August for Sun zenith angles between 30° and 70°.

the first scenario, increases in intensity and altitude. This thin layer is detected around 3000 meters and are in the same altitude of cloud formation. The lidar ratio in the second scenario, under cloud formation conditions is $LR = 80 \pm 16$ sr, presented in the right-bottom panel of figure 6. The lidar ratio changes can be associated to some changes in the aerosol optical properties and need a deep analysis in order to understand their role on the cloud formation. For the cloud formation scenario the RBR-AOD correlation is found to be low and need more detailed investigation, as presented in figure 5 and the equation 1.

4.1.2 Acquisition day - 12^{th} of September, 2016

The study case of 12^{th} of September is considered a clear-sky condition case as can be seen in the range corrected signal at 532 nm retrieved by the SPU lidar station presented in figure 7. For this cloud-free case, the RBR analysis in coincidence with the 532 nm AOD retrieved by the AERONET sunphotometer shows a strong correlation between RBR $\times$ AOD, as can be seen in figure 8 when compared to the first case study, under cloud conditions (figure 6). For the 12^{th} of September case the camera images retrieved cloud-free images and during some periods of the day there is the presence of scattered small clouds along the day. Although the scattered clouds are not detected by the SPU lidar station, the scattered radiation can be significantly affected by those clouds in the radiance registered by the camera. The backscatter profile retrieved during the last period of measurements, as can be seen in figure 7, was not affected by those scattered clouds as they are not in the beam path. The column average lidar ratio value between 15:12 and 15:42 UTC was found as 75 ± 15 sr, tuned by the AERONET's AOD at 532 nm value of 0.20.

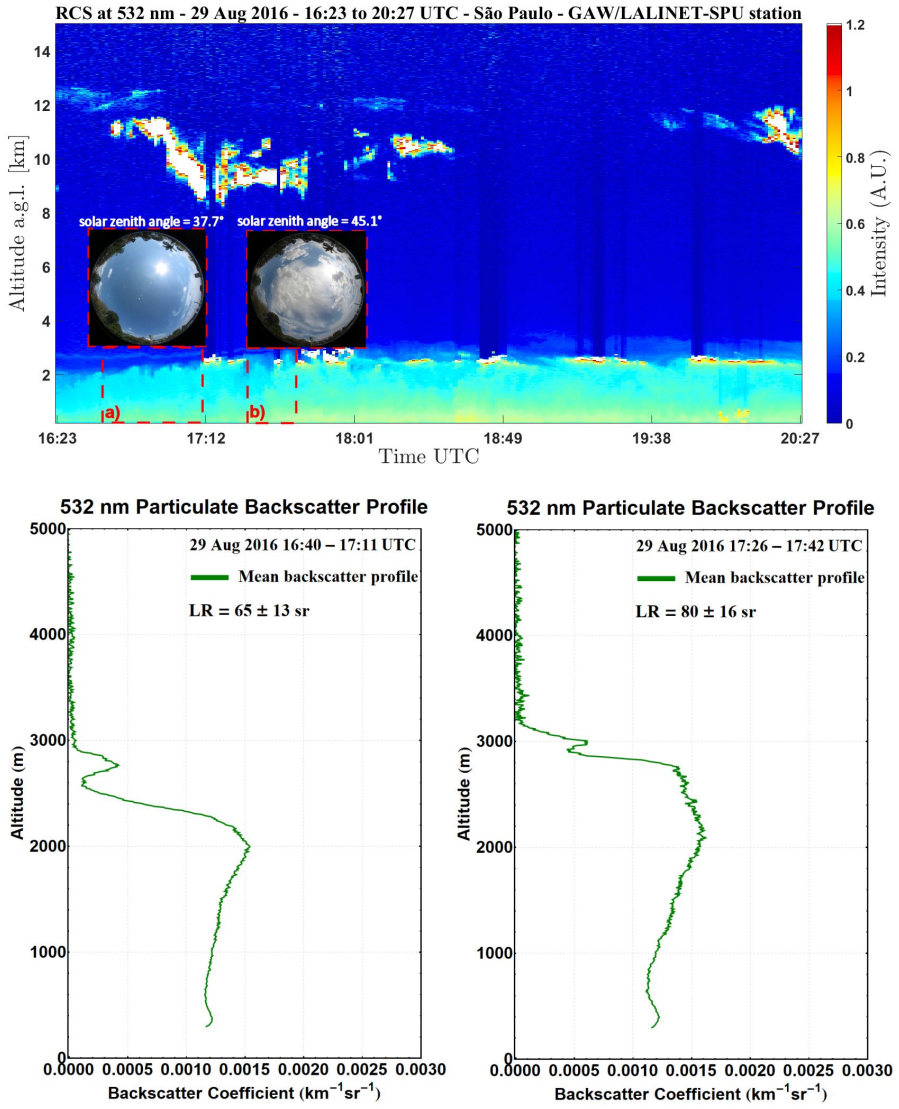

Figure 6. Range Corrected Signal (RCS) at 532 nm for 29^{th} of August of 2016 retrieved by SPU lidar station and the backscatter profiles at 532 nm for two scenes; a) before the clouds formation at the top of the PBL and, b) after and during the process of clouds detection.

The mean RBR values were correlated with the AOD values retrieved at 532 nm by the AERONET sunphotometer for closest period in time ($\approx$ 4 min) for both measurements. The RBR-AOD correlation for this particular case study was given by the equation 2. The cloud-free conditions allow to retrieve a strong correlation between Red-Blue ratio (RBR) and AOD values when compared to the first case considering the sky-clouded conditions.

$$RBR \;=\; -0.0349 \;+\; 2.7748\;\tau_{532} \tag{2}$$

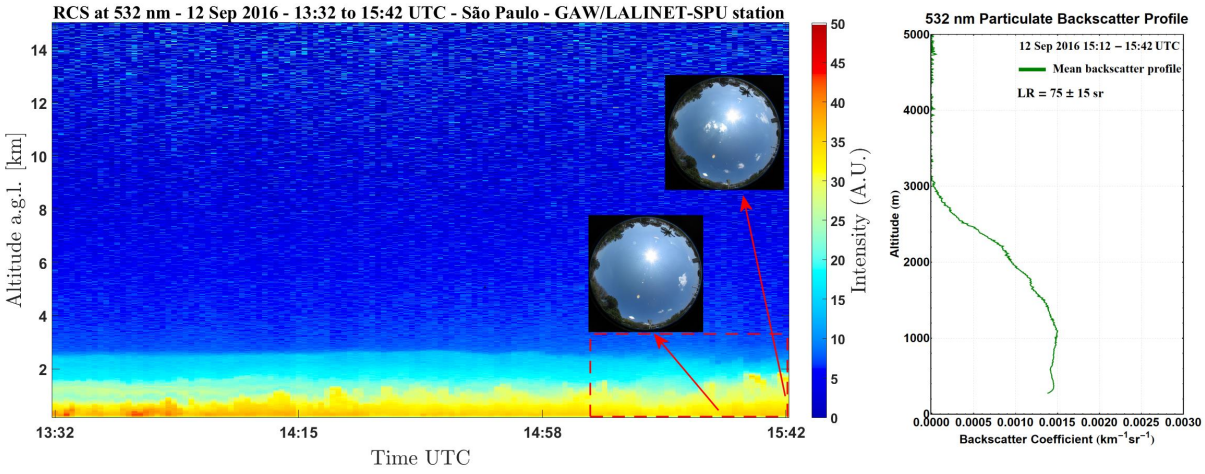

Figure 7. RCS at 532 nm for 12^{th} of September of 2016 retrieved by SPU lidar station and the backscatter profile at 532 nm for a clear-sky condition.

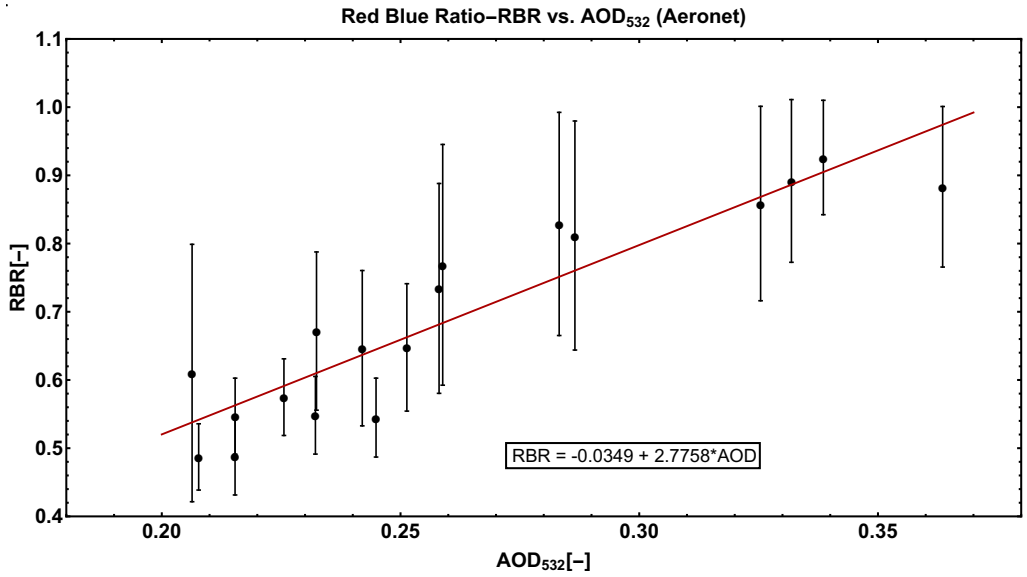

Figure 8. RBR-AOD at 532 nm correlation for 12^{th} of September for Sun zenith angles between 30° and 70°.

5. CONCLUSIONS

During August to September of 2016, a measuring campaign had been carried out in Metropolitan area of São Paulo, using a ground-based Raman Lidar system (GAW-LALINET SPU lidar Station), the AERONET sunphotometer network and an all-sky cloud camera in order to monitor the aerosol vertical distribution, cloud coverage and the correlation between image pixel classification parameters retrieved by all-sky camera and the AOD at 532 nm retrieved by AERONET. Two case studies presented with different atmospheric scenarios. The first one, measured on 29^{th} of August of 2016 was a cloud covered scenario and the second one a cloud-free scenario with a relative high load aerosol atmosphere, measured during 12^{th} of September of 2016. For the first scenario the correlation between Red-Blue ratio (RBR) and AOD at 532 nm is very low, probably because of the difficulty to retrieve the RBR values with high accurance or the contamination of AOD due to cloud scattering processes. However, the second scenario shows a strong correlation between RBR and AOD values.

These preliminary analyses show that a deep investigation, with a larger sky image database, is necessary to determine the role of aerosols in the cloud formation, for instance.

Acknowledgments

This work was supported by FAPESP (Fundação da Amparo à Pesquisa do Estado de São Paulo) through the project 15/12793-0 on the Research Program on Global Climate Change. The authors would like to acknowledge the Universidade Federal do Oeste da Bahia (UFOB) for the authorization for the process of teacher qualification of Jonatan J. da Silva. The authors also would like to acknowledge the Center for Lasers and Applications for supporting the project, and Paulo Artaxo, the PI of AERONET São Paulo site all AERONET sunphotometer network team.

REFERENCES

[1] Landulfo, E., Lopes, F. J. S., Guerrero-Rascado, J. L., and Alados-Arboledas, L., "Aerosol cloud interaction: a multiplatform-scenario-based methodology," *Proc.SPIE* **9645**, 9645–9645–10 (2015).

[2] Koehler, T. L., Johnson, R. W., and Shields, J. E., "Status of the whole sky imager database," (1991).

[3] Long, C. N., Sabburg, J. M., Calb, J., and Pags, D., "Retrieving cloud characteristics from ground-based daytime color all-sky images," *Journal of Atmospheric and Oceanic Technology* **23**(5), 633–652 (2006).

[4] Heinle, A., Macke, A., and Srivastav, A., "Automatic cloud classification of whole sky images," *Atmospheric Measurement Techniques* **3**(3), 557–567 (2010).

[5] Nakajima, T., Tonna, G., Rao, R., Boi, P., Kaufman, Y., and Holben, B., "Use of sky brightness measurements from ground for remote sensing of particulate polydispersions," *Appl. Opt.* **35**, 2672–2686 (May 1996).

[6] Landulfo, E., Papayannis, A., Artaxo, P., Castanho, A. D. A., de Freitas R. F. Souza, A. Z., Junior, N. D. V., Jorge, M., Sánchez-Ccoyllo, O. R., and Moreira, D. S., "Synergetic measurements of aerosols over são paulo, brazil using lidar, sunphotometer and satelite data during dry season," *Atmos. Chem. Phys.* **3**, 1523–1539 (2003).

[7] Landulfo, E., Papayannis, A., de Freitas, A. Z., Junior, N. D. V., Gonçalves, R. F. S. A., Castanho, A. D. A., Artaxo, P., Sánchez-Ccoyllo, O. R., Moreira, D. S., and Jorge, M. P. P. M., "Tropospheric aerosol observations in sao paulo, brazil using a compact lidar system," *Int. J. Rem. Sens.* **13**, 2797–2816 (2005).

[8] Guerrero-Rascado, J., Landulfo, E., Antuña, J., Barbosa, H., Barja, B., Bastidas, A., Bedoya, A., Da Costa, R., Estevan, R., Forno, R., Gouveia, D., Jiménez, C., Larroza, E., Lopes, F., Montilla-Rosero, E., Moreira, G., Nakaema, W., Nisperuza, D., Otero, L., Pallotta, J., Papandrea, S., Pawelko, E., Quel, E., Ristori, P., Rodrigues, P., Salvador, J., Sánchez, M., and Silva, A., "Towards an instrumental harmonization in the framework of LALINET: Dataset of technical specifications," *Proceedings of SPIE - The International Society for Optical Engineering* **9246**, 1–14 (2014).

[9] Guerrero-Rascado, J. L., Landulfo, E., na, J. C. A., de Melo Jorge Barbosa, H., Barja, B., Álvaro Efrain Bastidas, Bedoya, A. E., da Costa, R. F., Estevan, R., Forno, R., Gouveia, D. A., Jiménez, C., Larroza, E. G., da Silva Lopes, F. J., Montilla-Rosero, E., de Arruda Moreira, G., Nakaema, W. M., Nisperuza, D., Alegria, D., Múnera, M., Otero, L., Papandrea, S., Pallota, J. V., Pawelko, E., Quel, E. J., Ristori, P., Rodrigues, P. F., Salvador, J., Sánchez, M. F., and Silva, A., "Latin american lidar network (lalinet) for aerosol research: Diagnosis on network instrumentation," *Journal of Atmospheric and Solar-Terrestrial Physics* **138**, 112–120 (2016).

[10] Holben, B., Eck, T., Slutsker, I., Tanré, D., Buis, J., Setzer, A., Vermote, E., Reagan, J., Kaufman, Y., Nakajima, T., Lavenu, F., Jankowiak, I., and Smirnov, A., "AERONET - A Federated Instrument Network and Data Archive for Aerosol Characterization," *Remote Sensing of Environment* **66**(1), 1–16 (1998).

[11] Dubovik, O. and King, M. D., "A flexible inversion algorithm for retrieval of aerosol optical properties from Sun and sky radiance measurements," *Journal of Geophysical Research* **105696**(27), 673–20 (2000).

[12] Ghonima, M. S., Urquhart, B., Chow, C. W., Shields, J. E., Cazorla, A., and Kleissl, J., "A method for cloud detection and opacity classification based on ground based sky imagery," *Atmospheric Measurement Techniques* **5**(11), 2881–2892 (2012).

[13] Chauvin, R., Nou, J., Thil, S., Traoré, A., and Grieu, S., "Cloud Detection Methodology Based on a Sky-imaging System," *Energy Procedia* **69**, 1970–1980 (2015).

[14] Cloudcam, C. I. D. S. G., "Total sky camera find clouds software," *Automatic Sky Imaging System Manual Instructions* **3.4.0.0**, 1–74 (2015).

[15] Li, Q., Lu, W., and Yang, J., "A hybrid thresholding algorithm for cloud detection on ground-based color images," *Journal of Atmospheric and Oceanic Technology* **28**(10), 1286–1296 (2011).

[16] Shi, J. and Malik, J., "Normalized cuts and image segmentation," *IEEE Trans. Pattern Anal. Mach. Intell.* **22**, 888–905 (Aug. 2000).

[17] Li, Q., Lu, W., Yang, J., and Wang, J. Z., "Thin cloud detection of all-sky images using Markov random fields," *IEEE Geoscience and Remote Sensing Letters* **9**(3), 417–421 (2012).

[18] Souza-Echer, M. P., Pereira, E. B., Bins, L. S., and Andrade, M. A. R., "A simple method for the assessment of the cloud cover state in high-latitude regions by a ground-based digital camera," *Journal of Atmospheric and Oceanic Technology* **23**(3), 437–447 (2006).

[19] Carson, C., Belongie, S., Greenspan, H., and Malik, J., "Blobworld: Image segmentation using expectation-maximization and its application to image querying," *IEEE Transactions on Pattern Analysis and Machine Intelligence* **24**(8), 1026–1038 (2002).

[20] Neto, S. L. M., von Wangenheim, A., Pereira, E. B., and Comunello, E., "The use of Euclidean geometric distance on RGB color space for the classification of sky and cloud patterns," *Journal of Atmospheric and Oceanic Technology* **27**(9), 1504–1517 (2010).

[21] Lopes, F. J. S., Moreira, G. A., Rodrigues, P. F., Guerrero-Rascado, J. L., Andrade, M. F., and Landulfo, E., "Lidar measurements of tropospheric aerosol and water vapor profiles during the winter season campaigns over the metropolitan area of São Paulo-Brazil.," in [*Proc. SPIE, Lidar Technologies, Techniques, and Measurements for Atmospheric Remote Sensing X*], **9246** (2014).

[22] Klett, J. D., "Stable analytical inversion solution for processing lidar returns," *Appl. Optics* **20**, 211 (1981).

[23] Klett, J. D., "Lidar calibration and extinction coefficients," *Appl. Optics* **22**, 514 (1983).

[24] Fernald, F. G., "Analysis of atmospheric Lidar observations: some comments," *Appl. Optics* **23**, 652–653 (1984).